Chemical Engineering Journal 373 (2019) 973–984

Contents lists available at ScienceDirect

Chemical Engineering Journal

journal homepage: www.elsevier.com/locate/cej

A first evaluation of butanoic and pentanoic acid oxidation kinetics

Sylvain Namysl[a], Matteo Pelucchi[b,*], Olivier Herbinet[a], Alessio Frassoldati[b], Tiziano Faravelli[b], Frédérique Battin-Leclerc[a,*]

[a] Laboratoire Réactions et Génie des Procédés, CNRS, Université de Lorraine, ENSIC, Nancy Cedex, France
[b] CRECK Modeling Lab, Department of Chemistry, Materials and Chemical Engineering, Politecnico di Milano, Milan, Italy

HIGHLIGHTS

- First experimental datasets for butanoic and pentanoic acid oxidation.
- A new kinetic model was developed considering specificities induced by acids.
- The new model reproduces well the experimental data obtained.
- Considering any acid with an acid moiety and an alkane moiety is a valid hypothesis.

ARTICLE INFO

Keywords:
Butanoic acid
Pentanoic acid
Oxidation
Jet-stirred reactor
Detailed kinetic modeling

ABSTRACT

Despite the recent interest in large carboxylic acid oxidation due to their presence in pyrolysis bio-oils, their kinetics of pyrolysis and oxidation has not been experimentally addressed. For the first time, this paper reports a new set of experimental data for the oxidation in a jet-stirred reactor of two high molecular weight carboxylic acids: butanoic (butyric) and pentanoic (valeric) acids. This work was performed at 106.7 kPa (800 Torr) over a range of temperatures from 800 to 1100 K. The experiments were carried out under highly diluted conditions (inlet fuel mole fraction of 0.005) for three equivalence ratios: 0.5, 1 and 2. During this study a wide range of products has been identified and quantified from CO and CO_2 to C_5 species: 36 for pentanoic acid and 18 for butanoic acid. An interpretative kinetic model has been developed based on a recent theoretical study on the pyrolysis and oxidation of acetic acid (Cavalotti et al. PROCI, 37 (2019) 539–546) and on alkane rate rules (Ranzi et al. Combust. Flame, 162 (2015) 1679–1691). This new kinetic subset has been implemented in the CRECK kinetic framework covering the pyrolysis and oxidation of molecules from syngas up to heavy fuels, including PAHs formation. The mole fractions of fuel and product species were compared with results from model simulations over the experimental temperature range, providing reasonable agreement. A flow rate analysis allowed a better understanding of the most important degradation pathways of these acids, including a small contribution of low-temperature oxidation channels.

1. Introduction

Many reasons lie behind the interest in carboxylic acid oxidation chemistry. Oxygenated species, including those carrying acid functionalities, are very abundant in the tar released from biomass pyrolysis. Acetic acid, for example, is the major acidic components of bio-oils derived from biomass fast pyrolysis [1–3]. Fig. 1 presents the composition of three different bio-oils [2] and shows the importance of the acids in the composition (around 20% in this case).

New fuel formulations, meant to improve environmental impact and decrease energetic dependence on fossil fuels, are obtained by blending increasing amounts of biofuels (e.g. alcohols) into conventional fuels. Recent studies highlighted how the combustion of such fuels might introduce new issues for human health and that their impact on pollutant formation has not been fully assessed. In fact, new unregulated pollutants such as long chain aldehydes and organic acids may be formed in significant quantities during the combustion of these new fuels [4–6]. Therefore, according to the successive oxidation steps as alcohol > aldehyde > carboxylic acid, the accurate description of biofuel combustion has to properly account for the formation of relevant intermediates [7–9]. Furthermore, recent experimental and modeling studies on the low temperature oxidation chemistry of hydrocarbon fuels highlighted the importance of organic acid formation from alternative low temperature pathways of alkanes (e.g. Korcek

* Corresponding authors.
E-mail addresses: matteo.pelucchi@polimi.it (M. Pelucchi), frederique.battin-leclerc@univ-lorraine.fr (F. Battin-Leclerc).

https://doi.org/10.1016/j.cej.2019.05.090

Available online 16 May 2019

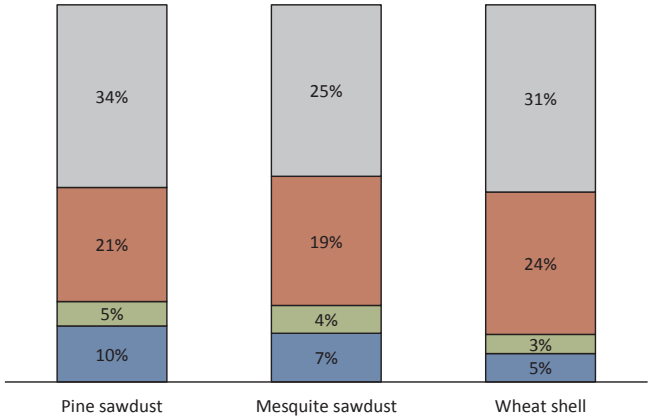

Fig. 1. Composition of three bio-oils. The sections are corresponding from the bottom to the top to alcohol (blue), aldehydes (green), carboxylic acids (red) and to the rest of the mixture (grey). (For interpretation of the references to colour in this figure legend, the reader is referred to the web version of this article.)

mechanism) [10–13]. From a fundamental kinetic perspectives, all of the above reasons highlight the need to properly assess the influence of the carboxyl functionality on the overall reactivity of different molecular weight acids.

Christensen and Konnov [14] recently reported the first experimental measurements of acetic acid laminar flame speeds, at P = 1 atm and T = 338–358 K. A kinetic model was also developed extending previous studies on formaldehyde and methanol [14,15] and the previous model developped by Battin-Leclerc et al. to simulate the formation of formic to propanoic acid for laminar premixed flame of propane [16]. Cavallotti et al. [17] recently investigated the gas-phase reactivity of acetic acid with ab initio methods, providing a solid basis to develop pyrolysis and oxidation kinetics of higher molecular weight acids as presented in this work. Rate constants for the unimolecular decomposition of acetic acid were determined with ab initio transition state based master equation, over a broad range of temperatures and pressures. The three main decomposition channels considered were $CH_3COOH \leftrightarrow CO_2 + CH_4$, $CH_3COOH \leftrightarrow CH_2CO + H_2O$, and $CH_3COOH \leftrightarrow CH_3 + COOH$. H-abstraction reactions by H, OH, OOH, O_2, and CH_3 from the carboxylic function and from the methyl group were also theoretically determined. Results were found to agree very well with experimental determinations of the rate constants. The updated CRECK model [18] provided good predictions in comparison with the limited amount of experimental data on acetic acid pyrolysis and oxidation [19,20,14,21].

Motivated by the absence of useful data for the development and the validation of butanoic and pentanoic acid gas phase oxidation kinetics in the literature, this work presents the first experimental datasets obtained for the above fuels. Experiments were performed in an atmospheric pressure jet-stirred reactor, over the temperature range 800–1100 K, for 0.5% fuel/O_2/He mixtures at varying equivalence ratios (φ = 0.5, 1.0, 2.0).

The unavailability of studies on the oxidation of acids can be explained by some experimental complexity. An issue is related to the relatively high boiling point of butanoic and pentanoic acids (436 K and 458 K, respectively) which are at the upper limit of our actual set-up capacities. The only experimental and kinetic modelling study for higher molecular weight acids ($C_n > 2$) was presented by Doolan et al. [22]. The authors investigated the thermal decomposition of propanoic acid in argon in a single pulse shock tube. Operating at temperatures ranging between 1100 K and 1500 K and at pressures P = 14–18 atm. Following a similar previous study specifically devoted to acetic acid [19] the authors systematically interpreted the acid pyrolysis kinetics by means of a kinetic model. Clark and co-workers [23] calculated barrier heights and high pressure limit rate constants for molecular decomposition pathways for a series of higher molecular weight acids, including propanoic and butanoic acids. Mendes et al. [24] performed theoretical calculations of H-abstraction reactions for a series of oxygenated compounds, including acetic and propanoic acids.

Moreover, stemming from the previous theoretical study on acetic acid this work also presents the first kinetic model for butanoic and pentanoic acids. This model is derived through analogy from both the recent assessment of acetic acid oxidation [17] and from alkane rate

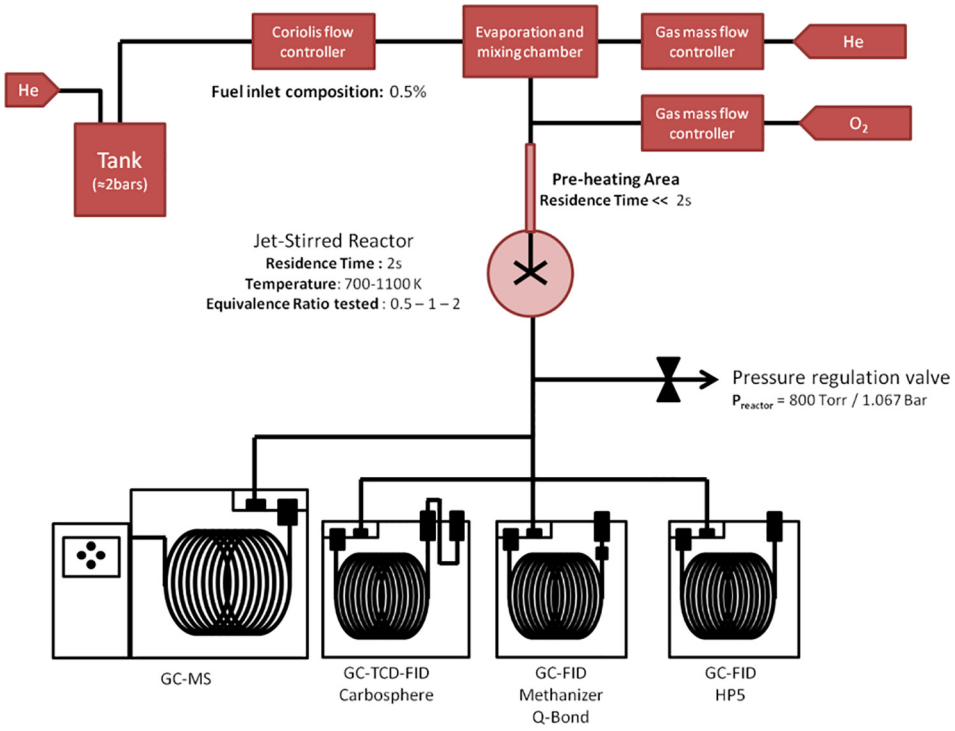

Fig. 2. Schematic of the JSR facility used in this study.

Table 1
Uncertainty quantification of the experimental setup.

Uncertainty sources	Uncertainty bounds
Temperature in the reactor	± 5 K
Temperature in the transfer line	± 7 K
Impurity of the fuels and the gases	< 1%
Fuel calibration (description below)	± 10%
Products calibration by effective carbon number method	± 10%
Products calibration with standards	± 5%
Flow rate of liquid fuel	± 1%
Flow rate of gases	± 0.5%
Residence time	± 2%

rules as implemented in the CRECK kinetic model [25,13].

2. Experimental method

The experimental set-up consists in an isothermal heated jet-stirred reactor (JSR) used at atmospheric pressure and coupled with gas chromatographic analyses. This setup was recently used to study the low-temperature oxidation of *n*-pentane [26] and of *n*-C_4-C_6 aldehydes [9]. Fig. 2 shows a schematic of the setup of the JSR with the analytical method used for this study.

The JSR consists of a fused silica sphere (volume 92 cm^3) equipped with four injection nozzles positioned in a cross at the center of the sphere [27,28]. This injection method ensures high turbulence in the reactor and leads to homogeneity in product concentration of the gas phase. Thanks to this homogeneity, the reactor can be assimilated to a perfectly stirred reactor working under steady-state conditions. To ensure thermal homogeneity, the isothermal JSR is preceded by a quartz annular preheating zone, in which the temperature of the gas is increased up to the reactor temperature. The gas residence time inside the annular preheater is very short compared to its residence time inside the reactor (a few percent); therefore the reactivity in this section can be considered as negligible. The heating is ensured by resistances (Thermocoax) carefully rolled to fit the reactor and the preheating zone shapes, which allows flexibility and swiftness in the heating of each area. Temperatures are measured by several K-type thermocouples: one is located in a glass finger inside the inlet cross for the actual reaction temperature measurement, and two are located between the resistances and the external wall of the reactor for the temperature control. The liquid fuel is stored in a pressurized tank. The liquid flow is measured by a Coriolis mass flow controller, which is connected to the valve of an evaporator. The liquid mass flow is constantly measured and a PID regulation assures the stability of the flow. The gas flows are measured with different gas flow controllers. The composition of the inlet mixture is calculated for each condition and fixed by the flows.

This study was performed between 700 K and 1100 K, at 106.7 kPa, at three equivalence ratios (φ = 0.5, 1.0, 2.0) for mixtures containing 0.5 mol% of fuel with dilution into He. The residence time in the reactor is taken equal to 2 s for all experiments. A variation in the residence time by a factor of 2, has a very limited effect as shown by Herbinet et al. [29] and the simulations on pentanoic acid results presented in Supplementary Materials. Butanoic and pentanoic acids were provided by Sigma Aldrich with a purity of 99%. Helium (99.999% pure) and oxygen (99.999%) were provided by Messer. Gas flow rates were controlled by mass flow controllers and the liquid flow rate by a Coriolis flow controller followed by a vaporization chamber maintained at a temperature 15 K above each fuel boiling point.

The outlet gas leaving the reactor was then transferred by a heated line maintained at 420 K to three gas chromatographs (GCs) to analyze the wide range of products formed by the reaction. Due to the temperature drop between the reactor exit and the transfer line, the gas can be considered as quenched and therefore the reactions stopped. The first chromatograph, equipped with a Carbosphere packed column, a thermal conductivity detector (TCD) and a flame ionization detector (FID), is used for the quantification of light-weight compounds like methane, ethylene, acetylene and ethane. The second chromatograph is fitted with a Q-Bond capillary column and a FID preceded by a methanizer and is used for the quantification of compounds containing from 2 carbon atoms, like acetylene or ethylene up to species containing up to 5 carbon atoms. The methanizer (nickel catalyst for hydrogenation) allows the detection of species like CO, CO_2 and CH_2O with a good sensitivity and increases the sensitivity for species containing oxygenated functional groups in a general manner. A third chromatograph equipped with a HP-5 capillary column is used for the detection of the heaviest compounds (C_{5+}) and for both fuels.

The identification of reaction products is performed using a gas chromatograph equipped with both type of capillary columns and coupled to a mass spectrometer (quadrupole). Calibrations are performed by injecting gaseous and liquid external standards when available. For species, which could not be directly calibrated with a standard, the effective carbon number method relying on the properties of the FID with respect of the structure of the molecule was used to obtain calibration coefficients from reference species calibrated using standards. Table 1 summarizes the uncertainties sources and their quantifications related to these experiments.

It is possible that condensation and physical adsorption occur on some surfaces in the manifolds (cold points, valve, gums). This could affect the quality of the results and solutions have to be found to limit those phenomena as much as possible. One solution consists in coating the surface with the fuel before the occurrence of any reactions [22]. In our case, the surfaces were constantly heated to limit the condensation of the heaviest compounds, so the controlled coating of the surfaces was not possible. Also some components in chromatographs are prone to adsorption; especially the sampling loop, and the inlet liner. Thus specific components of chromatographs were supplied by the Restek company and used for the experiments. An inlet liner made of deactivated silica (Topaz GC inlet liners) [30] and a surface-coated sampling loop (Sulfinert treatment) [31] were installed to minimize the occurrence of adsorption. All these equipments are also suitable for the study and analysis of other oxygenated compounds like alcohols or aldehydes so it does not modify the results we can get and let us the possibility to compare them with previous studies. The implementations described above lead to an maximum estimated relative error of 10% in the mole fraction of the fuel, which is however still higher than usual values previously obtained with the present setup for other fuels (i.e. 5%).

3. Experimental results

Fig. 3 compares measured fuel mole fraction profiles at different equivalence ratios. Results from kinetic simulations obtained with the model developed in this study are also plotted. As expected from the longer carbon chain, pentanoic acid is more reactive than butanoic acid throughout the equivalence ratio and temperature ranges here explored. Generally the onset of reactivity of butanoic acid is delayed of about 50–70 K with respect to pentanoic acid.

Fig. 4 compares the carbon based selectivities for butanoic and pentanoic acids for the stoichiometric case (φ = 1.0) of Fig. 3. Only the products exceeding 0.1% in terms of selectivity are here reported for clarity. The analysis was conducted at a fixed fuel conversion of 85%. As a consequence of the different reactivity mentioned above, this extent of consumption is obtained at two different temperatures for the two fuels. Namely, this analysis was carried out at 950 K for butanoic acid and at 900 K for pentanoic acid. For these two temperatures, the carbon loss is around −1% and 17% for butanoic and pentanoic acid respectively.

For both fuels, beside the expected high yields of ethylene, CO and CO_2, ~8% of the fuel carbon are converted to propene. Notable mole fractions of 1-butene are also observed. Due to the C_4 skeleton of butanoic acid, 1-butene can only be formed through recombination

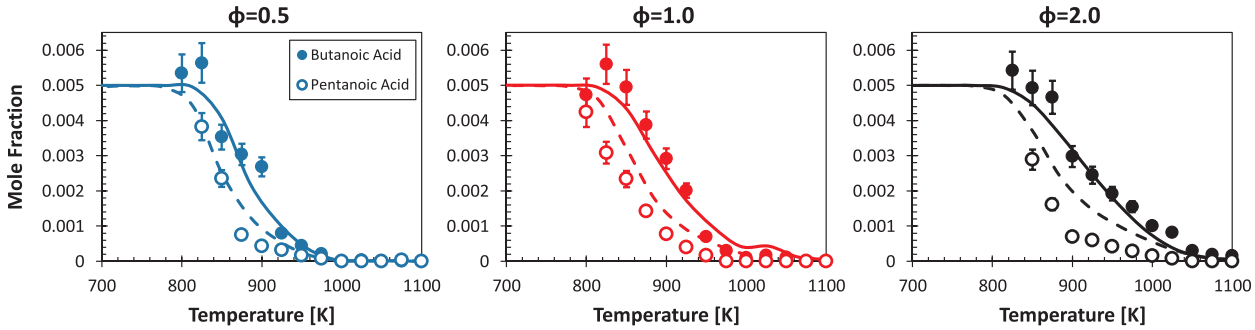

Fig. 3. Comparison of experimental fuel mole fraction profiles (symbols) and model simulations (lines). Oxidation of 0.5% butanoic (full symbols and full lines) or pentanoic acid (open symbols and broken lines)/O_2/He mixtures in an isothermal JSR, φ = 0.5, 1.0, 2.0, P = 1.05 atm, τ = 2.0 s. 10% error bars are reported.

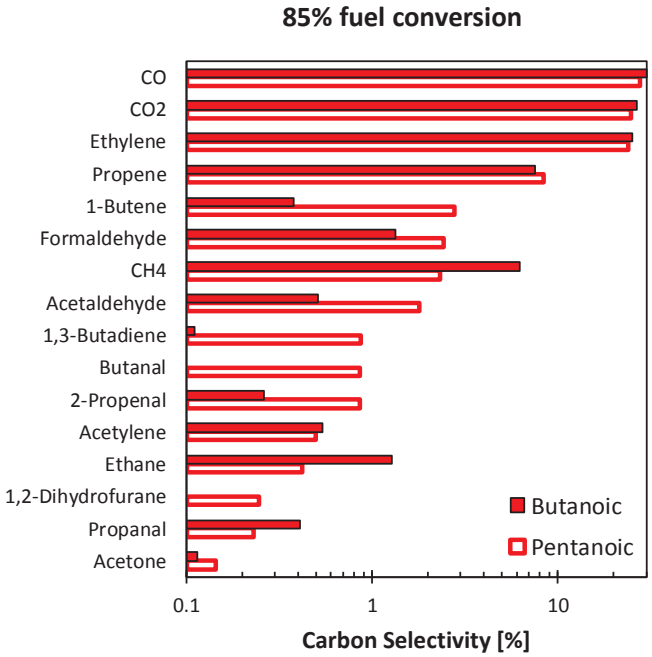

Fig. 4. Experimental comparison of carbon selectivities to products at 85% fuel conversion in the oxidation of butanoic and pentanoic acids in stoechiometric conditions (φ = 1). (950 K for butanoic acid, 900 K for pentanoic acid).

reactions of relatively stable radicals (e.g. CH_3 + aC_3H_5). In the case of pentanoic acid instead, 1-butene is formed mainly by the β-scission decomposition reaction of the fuel radical carrying the unpaired electron on the β carbon atom as discussed in Section 5. Butadiene is formed by H-abstraction and successive decomposition reactions of the unsaturated pentenoic acid mostly formed by fuel radicals β-scission decomposition reactions and interactions with molecular oxygen abstracting an H-atom. Methane is mostly formed through H-abstraction reactions (e.g. CH_3 + RH ↔ R + CH_4) from fuel and the recombination of two methyl radicals produces ethane (CH_3 + CH_3 + M ↔ C_2H_6 + M). Ethane is converted to ethylene and acetylene by successive dehydrogenation reactions. A more detailed discussion of reactive fluxes is provided in Section 5 (Figs. 11 and 14).

CH_2O and CH_3CHO are the most abundant aldehydes formed in the oxidation of both fuels. The higher oxygen content in the pentanoic acid mixture, for a given fuel concentration, justifies the higher amounts of formaldehyde and acetaldehyde. *n*-Butanal at high temperatures (T > 1000 K) if formed by successive dehydrogenation/oxidation reactions of 1-butene, therefore reflecting its relative amount in the two cases, while at low temperatures its formation mostly occurs through a Waddington like decomposition of the peroxy radical formed from the α-radical addition to O_2 as discussed in Section 4.5. The same pathway justifies most of the formation of propanal in butanoic acid oxidation.

4. Kinetic model

This section describes the development of the kinetic model for higher molecular weight acids. Moving from the evaluation of bond dissociation energies and thermodynamic properties of relevant species (Section 4.1), the derivation of rate constants for the different reaction classes needed to model pyrolysis, high and low temperature oxidation of long chain carboxylic acids is discussed in the followings.

4.1. Thermochemistry and bond dissociation energies (BDEs)

Thermodynamic properties for butanoic acid, pentanoic acid and their radicals were estimated using software THERGAS [32] that implements Benson's group additivity rules [33]. From the calculated enthalpies of formation, it is possible to estimate the bond dissociation energies (BDEs) reported in Fig. 5 for acetic, propanoic, butanoic and pentanoic acids. As recently reported by Pelucchi et al. [5], the evaluation of BDEs provides useful guidelines for the development of a kinetic model based on analogy rules. This analysis clearly highlights the extent to which the oxygenated functional group influences vicinal bonds. In other words, as also discussed by Heufer et al. [34] for long chain alcohols oxidation and represented in Fig. 5, it is possible to

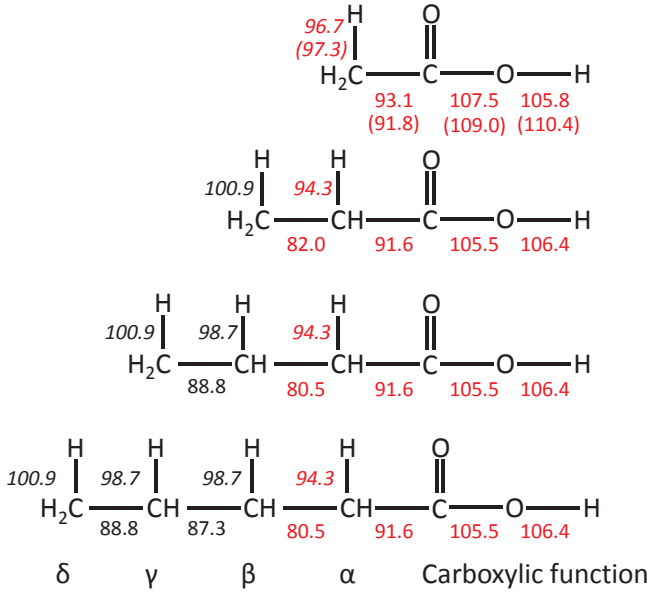

Fig. 5. Bond dissociation energies for a series of acids: acetic, propanoic, butanoic and pentanoic (C—H bonds in italics), calculated using bond additivity. Values in red represent acid specific moieties, black values represent alkane-like moieties. Values in parentheses are from Cavallotti et al. [17].

assume the acid molecule as composed of an acid specific moiety (BDE values in red) and an alkane-like moiety (BDE values in black). In fact, the effect of the carboxylic functional group (R−(C═O)−OH) vanishes after the C_β-H bonds (italics in Fig. 5) and after the C_β-C_γ bonds of butanoic and pentanoic acids. Indeed, C−H bonds farther away from the carboxylic function present the same values of primary (100.9 kcal/mol) and secondary bonds (98.7 kcal/mol) in alkanes. Similar analogies are also valid for C−C bonds far from the oxygenated group involving two primary carbons (88.8 kcal/mol) or a primary carbon bonded to a secondary carbons (87.3 kcal/mol).

Concerning the accuracy of thermochemistry estimation based on group additivity methods, Fig. 5 also reports the bond dissociation energies of acetic acid as in the recent theoretical study of Cavallotti et al. [17]. Reasonable agreement (i.e. within 2 kcal/mol) can be observed for every bond exception made for the terminal O−H bond of the carboxylic moiety, where our estimation differs of 4.6 kcal/mol from the calculated values. The comprehensive review of Luo et al. [35] provides a value of 112 ± 3 kcal/mol for this bond. The same bond for higher molecular weight acids is slightly weaker and the computed BDE of 105.5 kcal/mol is only 0.6 kcal/mol smaller than the value estimated by Denisov et al. [36].

Due to resonance stabilization, the most stable radicals with the same carbon skeleton of the parent acid is that carrying an unpaired electron on the carbon atom closest to the carboxylic function, with a BDE of ~97 kcal/mol for the primary position in acetic acid and 94.3 kcal/mol for secondary positions in higher molecular weight acids. In both cases, the resonance induces a stabilization of ~4 kcal/mol compared to an alkane-like primary or secondary radical derived from a C_α−H bond cleavage. The favored radical decomposition is that involving C_β-C_γ bonds, as it leads to the formation of the stable radical *CH2−(C═O)−OH that is also resonance stabilized. For primary-secondary bonds close to the functional group (C_α−C_β), dissociation energies are 80.5 kcal/mol, which is 1.5 kcal/mol lower than secondary-secondary bonds in butanoic and pentanoic acids. This observation is consistent with the energy difference between a primary-primary and a primary-secondary C−C bond in alkanes (88.8 vs 87.3 kcal/mol). BDEs for C_{COOH}-C_α bonds leading to the formation of the unstable HOCO radical (*(C═O)−OH) and a C_{n-1} alkyl radical are 91.5 kcal/mol, which is 4.3 kcal/mol stronger compared to similar bonds in alkanes.

Based on the above observations it is possible to derive a kinetic model based on analogies. Rate constants for the different reaction classes can be treated according to the recent work of Cavallotti et al. [17] for acetic acid when referring to the acid specific moiety. Concerning the remaining part of the molecule, established rate rules for alkanes [25,13] are adopted in this work. This model in CHEMKIN format, together with thermochemical data, is provided in Supplementary material.

4.2. Unimolecular decompositions

Acetic acid mostly decomposes through molecular decomposition pathways (E_a ~ 71–74 kcal/mol) due to the much larger activation energies of unimolecular initiation reactions (E_a ~ 93–110 kcal/mol) [17]. However, conventional radical initiation pathways are more important for acids with a longer carbon chain, as the effect of the carboxylic substitution vanishes. In particular, while a limited contribution is expected from the strong C−O and O−H bonds, the weak C_α−C_β can overcome or compete with decarboxylation and dehydration reactions.

Fig. 6 compares the rate constants for molecular decarboxylation and dehydration reactions of different carboxylic acids as reported by Cavallotti et al. [17] (acetic acid), Clark et al. [23] (acetic, propanoic and butanoic acids) and Doolan et al. [22] (acetic and propanoic acids). Decarboxylation reactions of the C_n acid produces CO_2 and a C_{n-1} alkane molecule. Dehydration reactions produce H_2O, and an alkyl ketene (R−(CH)═C═O). Specific subsets to describe the primary decomposition and oxidation reactions of ethylketene (C_2H_5(CH)═C═O) and propylketene (C_3H_7(CH)═C═O) have been introduced based on analogy with ketene and methylketene kinetics. From the systematic investigation of Clark et al. [23] the difference between dehydration reaction rate constants of acetic, propanoic and butanoic acids is within a factor of 2, with a surprising trend as propanoic > butanoic > acetic. However, the observed differences are well within the uncertainties of the adopted theoretical methods, therefore we assume the same rate constants proposed by Cavallotti et al. [17] for the molecular decomposition reactions of higher molecular weight acids. Despite the hierarchical development of kinetic subsets for higher C_4 and C_5 acids requires the inclusion of molecular and unimolecular initiation reactions, it has to be noted that under the experimental conditions presented in this work these reactions do not play a dominant role. Better insights on their importance can be obtained from an experimental investigation of butanoic and pentanoic acids in pyrolytic conditions.

BDEs of C−C, C−O, and C−H discussed above are used to estimate unimolecular decomposition reactions, responsible for radical chain initiation. Because of the microscopic reversibility principle, the rate constant of initiation reactions are derived from the rate constant of reverse barrierless radical recombination reactions. The most favored initiation reactions are those involving the lower BDEs and in particular those occurring through C_α−C_β bond breaking, due to its relatively low activation energy (80.5 kcal/mol) and the high frequency factor that is typical of initiation reactions ($A = 10^{17}\ s^{-1}$). Differently from acetic acid [17], the radical decomposition pathways account for > 80% of the total unimolecular decomposition of butanoic and pentanoic acids. Due to the high bond dissociation energies in acetic acid instead, molecular pathways were found to be the dominant decomposition channels.

4.3. H-abstraction reactions

H-abstraction reactions are relevant to unravel the selectivity to different products. Rate constants of the generic reaction: R· + R′H ↔ R′· + R H depend on the properties of the abstracting radical and the type of hydrogen to be abstracted [32]. In other words, the BDEs of the different C−H bonds to some extent reflect the likelihood of one H-atom to be abstracted. While this is generally verified for hydrocarbon fuels (alkanes, cycloalkanes and aromatics), hindered rotor effects, hydrogen bonding interactions and specificities of transition states [17] can be peculiar in oxygenated molecules. Stemming from the relative strength of the different C−H bonds in butanoic and pentanoic acids, one would indeed expect the relative importance to decrease as C_α−H > C_β−H > $C_{\gamma,\delta}$−H > O−H. Starting from a simpler example, the H-abstraction from the primary C_α site in acetic acid should be faster than the abstraction from a secondary position in alkanes. Fig. 7 compares the results from Cavallotti et al. [17] for H-abstraction reactions by H and OH from the α site in acetic acid with reference rate parameters for primary and secondary positions in alkanes [25].

The interactions with the carboxylic function inhibit the H-abstraction making it a factor of ~3–4 lower than an alkane primary position over the temperature range of interest.

According to the approach of Ranzi et al. [37] rate rules for the different R· abstracting radicals in the CRECK model are expressed as:

$$k_R(T) = n_H C_{SiteH}(T) k_{ref,R}(T) = n_H C_{SiteH}(T) A_{ref,R} T^2 exp\left(-\frac{E_{ref,R}}{RT}\right)$$

where the rate rules rely on reference frequency factors and activation energies of each H abstracting radical ($k_{ref,R}(T)$), on a per site primary alkane H-atom basis. The rates are then corrected to account for the number of H atoms and the correction term ($C_{SiteH}(T) = exp(-E_{SiteH}/RT)$) is obtained from the bond dissociation energy (or the heat of reaction), through an Evans-Polanyi relationship [38]. Following the same approach, the rate constants from Cavallotti et al. [17] can be corrected to obtain an estimate of the rate parameters

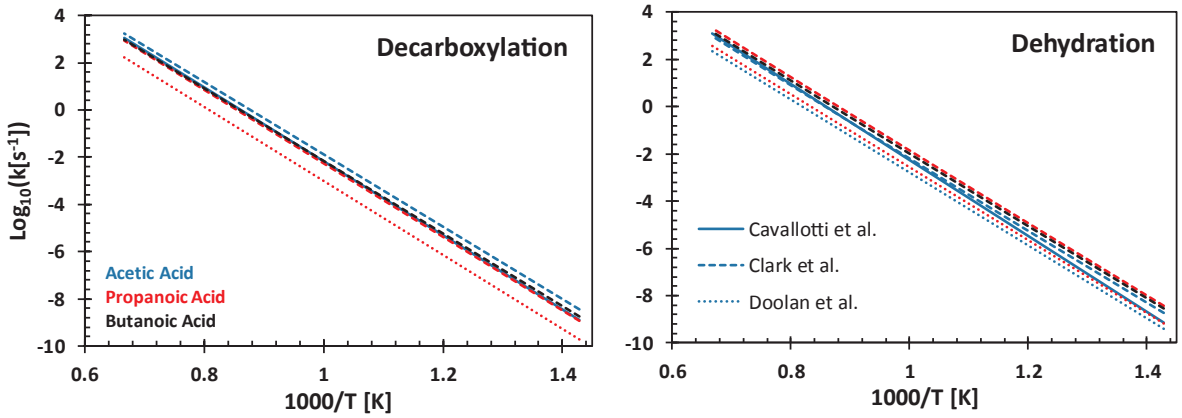

Fig. 6. Rate constants for molecular decarboxylation reactions (left) and dehydration reactions (right) for acetic acid (blue), propanoic acid (red) and butanoic acid (black). Literature values are from [22,23,17].

for H-abstractions from secondary α sites in higher molecular weights acids (propanoic, butanoic and pentanoic). The rate is modified reducing the activation energy by 2300 cal/mol ($E_{SiteH} = -2300$ cal/mol) and accounting for the different numbers of H-atoms available on the site. To prove the reliability of this approach, Fig. 8 compares the corrected values with theoretical calculations of Mendes et al. [24] for H-abstractions by H and OH on propanoic acid. Mendes et al. [24] estimated an uncertainty of a factor of ~2.5 in their calculations. For the case R = H, maximum deviations are within a factor of ~2.7. An even better agreement is obtained for R = OH, with maximum deviations within a factor of ~1.8.

Provided the above agreement, the same approach is applied for the remaining main abstracting radicals: HO_2, CH_3, O_2. The rate constants for H-abstractions from the hydroxyl function (O—H) of butanoic and pentanoic acids are adopted directly from the work on acetic acid [17]. Concerning the remaining alkane-like part, we adopt the reference values of alkanes for primary and secondary positions. A comparison between these reference parameters for the primary alkane positions with the calculations of Mendes et al. [24] for propanoic acid also provides good agreement (~2.5) supporting the validity of the assumption of an alkane-like moiety as resulting from the BDEs assessment (Fig. 4).

Fig. 9 shows the relative selectivities to the different sites for H-abstraction reactions by OH on butanoic acid, as computed from the values adopted in this work on a per H-atom basis. As expected from the strong bond energy, the selectivity of H-abstraction from the hydroxyl group of the carboxylic function only accounts for a few percentage at

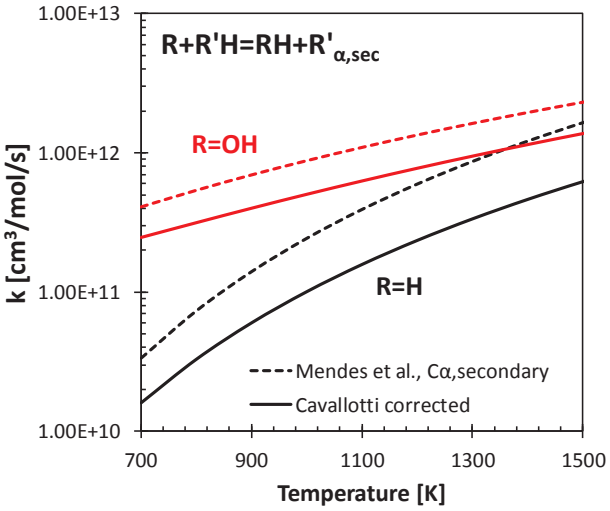

Fig. 8. comparison between calculated values from Mendes et al. [24] for H-abstractions from the α-site of propanoic acid and values adopted in the kinetic model derived by correcting the rate constants from Cavallotti et al. [17] for acetic acid.

very high temperatures for the case R = OH (10% at 1500 K). 29–43% selectivities are observed for H-abstractions from the secondary position in α. H-abstractions from the secondary alkane-like position (β) shows the higher yields at low temperatures (40%) decreasing to 23%

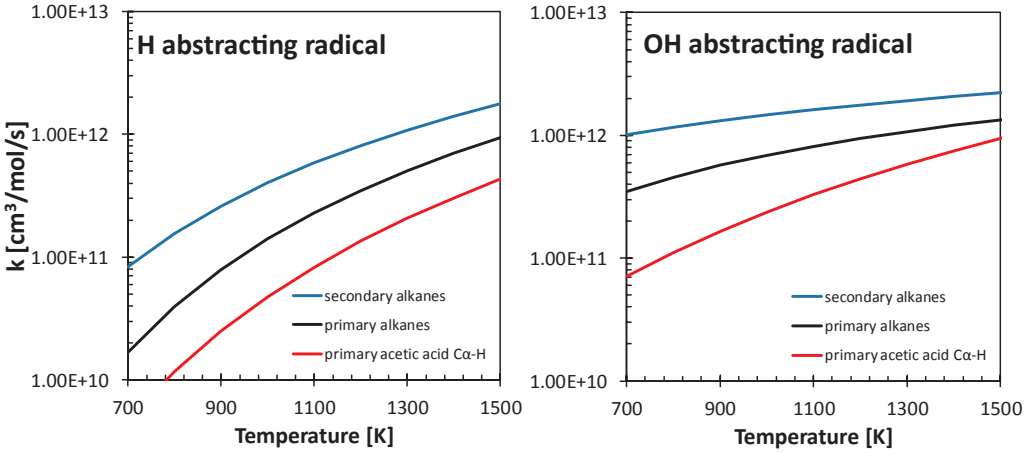

Fig. 7. Comparison between H-abstraction rate constants for primary position in acetic acid [17] and primary and secondary positions in alkanes [25]. Left panel: R = H, right panel: R = OH.

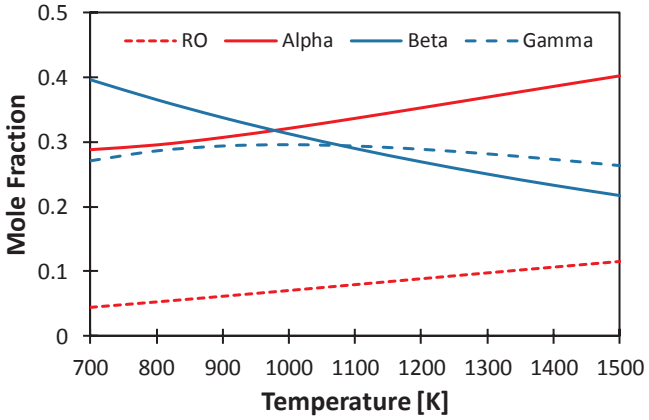

Fig. 9. Relative selectivities to the different H-abstraction sites on butanoic acid on a per H-atom basis. Abstractor R = OH.

at 1500 K. Concerning the primary position γ, ~30% yields is observed throughout the temperature range.

4.4. Radical decompositions/isomerizations

The fuel radicals derived from H-abstraction reactions can either decompose through beta-scission reactions to form a saturated bond and a smaller radical, or isomerize to another radical. Beta-scission reactions can break a C—H bond or a C—C bond. Rate constants for these reaction classes are based on the alkanes rate rules from Ranzi et al. [39] taking into account the differences in bond dissociation energies and the formation of resonance stabilized radicals (α-radicals) from H-abstractions. The previous study from Cavallotti and co-workers [17] highlighted the importance of secondary chemistry of the resonance stabilized α radical (*CH_2(C═O)—OH) in acetic acid for the predictions of the laminar flame speeds measured by Christensen and Konnov [14]. Preliminary evaluations by Cavallotti et al. [17] have been considered in this study to describe the decomposition reactions of these radicals and their interactions with H atoms.

Concerning β-decomposition reactions of α-radicals, rate constants are obtained by increasing the reference activation energy for beta-scission reactions (~30 kcal/mol [39]) by 2 kcal/mol in the case of butanoic acid producing methyl radical and acrylic acid (C_2H_3(C═O)—OH), and by 1 kcal/mol in the case of pentanoic acid where ethyl radical is produced instead. The decomposition reactions of the remaining fuel radicals to form unsaturated species and an alkyl radical, or to form unsaturated acids (butenoic and pentenoic acids) and H, are based on analogy with alkane rate rules [25]. Specific subsets to describe the pyrolysis and oxidation of butenoic and pentenoic acids have also been included. According to a similar approach, the carboxylic function is treated in analogy with saturated acids, while the unsaturated carbon skeleton is treated according to alkene kinetics already implemented in the CRECK model (i.e. propene and butenes). Interactions of fuel radicals with O_2 can also lead to the formation of unsaturated acids with the same carbon skeleton as the fuel, according to the generic H-abstraction reaction $O_2 + R_n = HO_2 + C_{n,unsaturated\ acid}$. To constrain the number of species in the kinetic model, only one butenoic acid and one pentenoic acid are accounted for to represent all the isomers. The reader is referred to the Supplementary Material for a detailed list of lumped species.

4.5. Low temperature lumped kinetics

Lumped low temperature pathways have been also included in the kinetic subsets here developed. The contribution to the low temperature branching pathways of the carboxylic function can be neglected due to the strong BDE of the O—H bond and due to the lack of H-atoms on the central carbon (R—(C═O)—OH). As can be noted from Fig. 3, neither low temperature reactivity nor NTC (negative temperature coefficient) can be seen under the experimental conditions investigated in this study. For these reasons, aiming at a first simplified description of acid low/intermediate temperature kinetics, the low temperature pathways and their rate constants are considered to be analogous to those in propane for butanoic acid and to those of *n*-butane for pentanoic acid. The anticipated onset of pentanoic acid reactivity observed in Fig. 3 is explained by a higher production of HO_2 radicals, undergoing the usual pathway of termination ($HO_2 + HO_2 = H_2O_2 + O_2$) followed by H_2O_2 decomposition triggering the reactivity ($H_2O_2 + M = OH + OH + M$). According to the same approach already reported for alcohols [6], a detailed approach is kept until the first addition of the different fuel radicals to O_2, forming one lumped peroxy radical species that undergoes low temperature and NTC pathways. The reader is referred to the Supplementary Material for a detailed list of lumped species.

Overall, the CRECK model adopted in this work (503 species and 17,025 reactions) implements a C_0-C_3 core subset obtained by coupling the H_2/O_2 and C_1/C_2 from Metcalfe et al [40], C_3 from Burke et al [41], and heavier fuels from Ranzi et al. [42,25]. It covers from syngas to heavy diesel fuel pyrolysis and combustion, including PAH formation [43] as well as a new subset of reactions for oxygenated aromatics of interest as bio-oils surrogates components [44]. The thermochemical properties for species not specifically belonging to the acid subset were adopted, when available, from the ATcT database of Ruscic [45] or from Burcat's database [46].

5. Comparison with experimental data and model validation

This section presents comparisons between experimental measurements and model simulations. Simulations of the jet-stirred reactor were performed with the dedicated solver included in the OpenSMOKE + + framework of Cuoci et al. [47]. Fig. 10 compares model simulations and experimental results for fuel conversion and mole fractions of the main products for butanoic acid oxidation at three equivalence ratios (φ = 0.5, 1.0, 2.0). The model is able to predict well the reactivity of the fuel for all the equivalence ratios with the onset of conversion at ~830 K for all the conditions. In general intermediate species are largely underestimated at the highest temperatures (T > 1000 K) for the rich case although CO and CO_2, covering the most of the carbon balance, are correctly reproduced. The largest deviations are observed for acetaldehyde (CH_3CHO), where predicted yields are ~4 times lower than the experimental measurements. Acetaldehyde is mostly produced by interactions of O/OH/O_2 with propene and propene radicals (e.g. *CH═CH—CH_3), whose kinetics are outside the scope of this study.

As mentioned in Section 3, propanal is largely produced by a Waddington-type mechanism [48,49] summarized in Fig. 11. The same rate constant as that adopted for the Waddington mechanism in alcohols [6] is here assumed.

Fig. 12 reports a reactive flux analysis for butanoic acid. At T = 900 K, φ = 1.0, corresponding to ~45% fuel conversion, butanoic acid is almost entirely consumed by H-abstraction reactions. The main abstracting radical is OH, but also methyl radical, which contributes to a lower extent to the fuel consumption. ~33% of the fuel produces the primary γ radical that is largely decomposed through β–scission to form ethylene and the resonance stabilized *CH_2(C═O)—OH radical. A limited flux (~2%) corresponds to the radical addition to O_2, forming a lumped peroxy radical (RO_2). 25% of the fuel forms the secondary β radical, that decomposes (20.3%) to propene and HOCO, or adds to oxygen to a lower extent forming RO_2. A larger amount of peroxy radicals is produced by the radical carrying the unpaired electron in α, as its β decomposition forming propenoic acids (C_2H_3COOH) is energetically slightly less favored due to methyl elimination. Of the overall flux leading to RO_2, only a minor extent isomerizes to QOOH that is mostly decomposed to butenoic acid, not propagating the low-

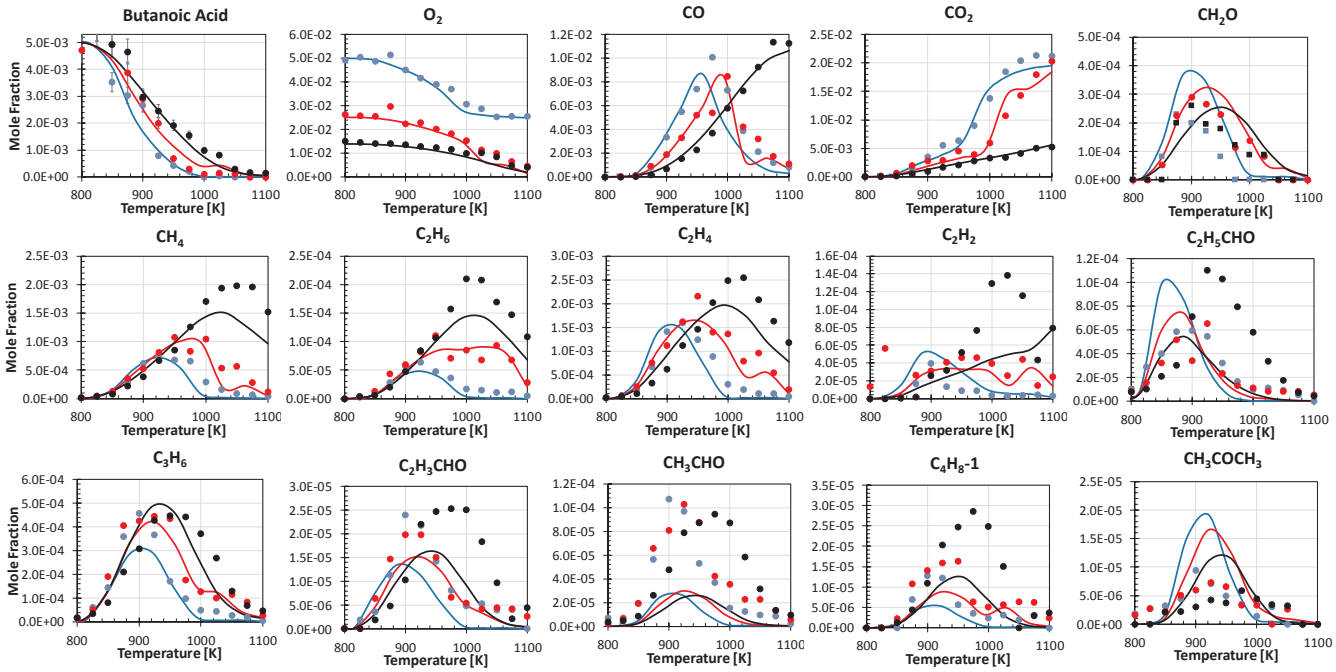

Fig. 10. Butanoic acid oxidation in JSR for all the equivalence ratios. Comparison between experimental (symbols) and predicted (lines) mole fractions (blue: φ = 0.5, red: φ = 1 and black: φ = 2). 10% error bars are reported for fuel mole fractions. Uncertainties for other species are discussed in Section 3. (For interpretation of the references to colour in this figure legend, the reader is referred to the web version of this article.)

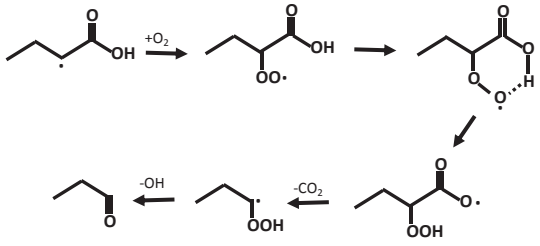

Fig. 11. Waddington-type mechanism explaining the formation of C_{n-1} aldehydes from the oxidation of C_n carboxylic acids at low/intermediate temperatures.

temperature branching pathway by means of a second addition to O_2. The Waddington-type mechanism proposed above only accounts for 0.8% of the overall flux, corresponding to 20% of the fate of RO_2 radicals.

Fig. 13 compares model predictions and experimental measurements of intermediate and product species in pentanoic acid oxidation, at three equivalence ratios (φ = 0.5, 1.0, 2.0). The model correctly capture the onset of fuel reactivity, occurring at temperatures lower than 800 K. Delays of ~10–20 K and ~20–30 K are observed in terms of fuel conversion for the stoichiometric (φ = 1.0) and the rich (φ = 2.0) cases, respectively. However, the reactivity seems to be correctly predicted when referring to O_2, CO and CO_2 profiles. Some

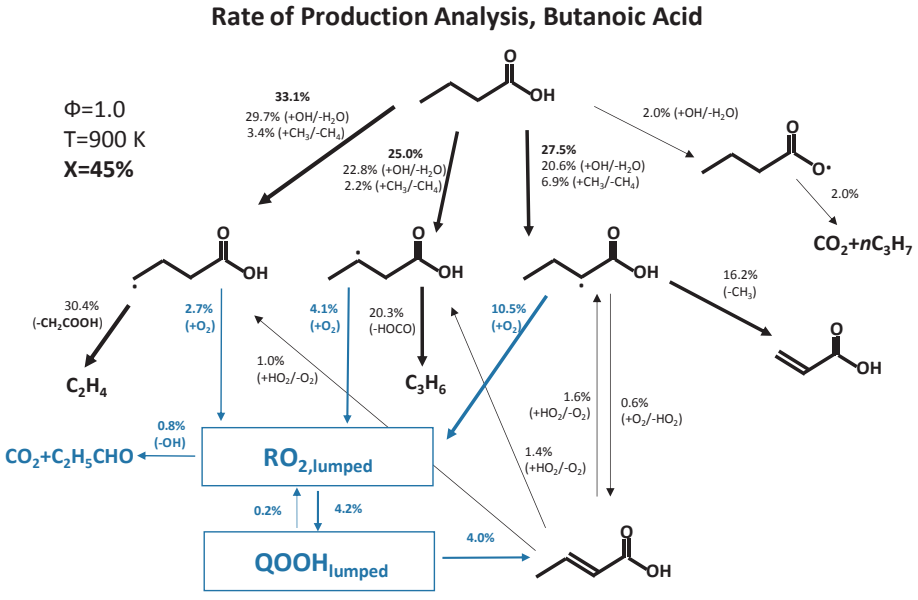

Fig. 12. Rate of production analysis of 0.5% butanoic acid/O_2/N_2 oxidation at T = 900 K, φ = 1.0 and 45% conversion. Threshold for contribution is 2% flux.

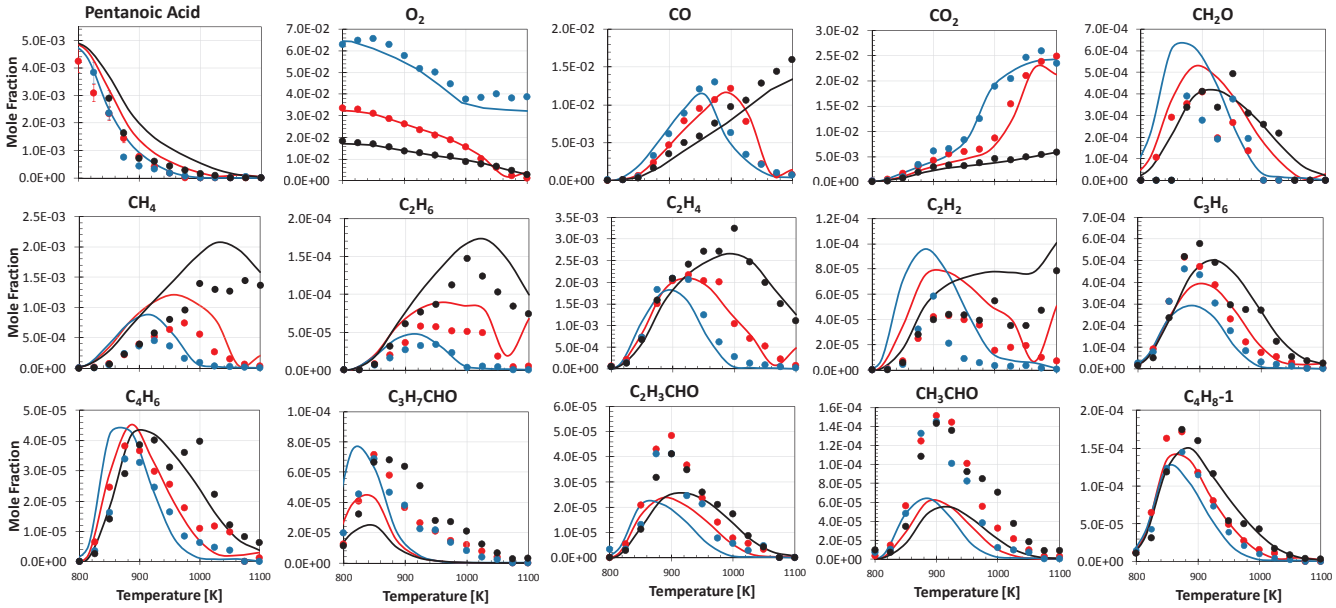

Fig. 13. Pentanoic acid oxidation in JSR for all the equivalence ratios. Comparison between experimental (symbols) and predicted (lines) mole fraction (blue: φ = 0.5, red: φ = 1 and black: φ = 2). 10% error bars are reported for fuel mole fractions. Uncertainties for other species are discussed in Section 3. (For interpretation of the references to colour in this figure legend, the reader is referred to the web version of this article.)

controversial result is observed also in the case of methane and ethane yields with the model predicting an earlier formation (i.e. ~ 40 K earlier). Methyl radical controls both methane and ethane formation via H-abstractions from the fuel (CH_3 + Fuel = CH_4 + FuelRadical), and methyl radicals recombination ($CH_3 + CH_3 + M = C_2H_6 + M$). Provided that the same rate constants for H-abstraction by CH_3 are implemented for butanoic and pentanoic acids, this disagreement is unexpected. Acetylene is mostly formed by successive dehydrogenations of ethane ($C_2H_6 \rightarrow C_2H_4 \rightarrow C_2H_2$), and is also slightly overestimated (~1.5 times). The Waddington-type mechanism allows a correct quantitative prediction of *n*-butanal yields; despite the predicted peaks occur ~20–30 K before those experimentally observed.

Fig. 14 reports a reactive flux analysis for pentanoic acid. At T = 865 K, φ = 1.0, corresponding to ~45% fuel conversion, pentanoic acid is almost entirely consumed by H-abstraction reactions leading to the formation of δ- (19.7%), γ- (37.9%), β- (15.7%) and α- (15.1%) radicals. Beside OH and CH_3, HO_2 radicals also contribute to fuel consumption via H-abstractions. The lower temperature at which the same conversion (X = 45%) is reached with respect to butanoic acid (Fig. 12) justifies the higher HO_2 concentration and therefore its contribution to fuel consumption. The longer carbon chain justifies the higher importance of radical isomerization reactions, with an overall ~4.5% flux of δ-radicals isomerizing to α-radicals, via a 5-membered ring transition state. Ethylene is mostly formed by the decomposition of δ-radical. *CH_2CH_2−(C═O)OH radical is formed together with ethylene, and its decomposition (*CH_2CH_2−(C═O)OH = C_2H_4 + HOCO) leads to another ethylene molecule and HOCO radical. The fuel radical in γ decomposes to propene and *CH_2(C═O)−OH, or to pentenoic acid

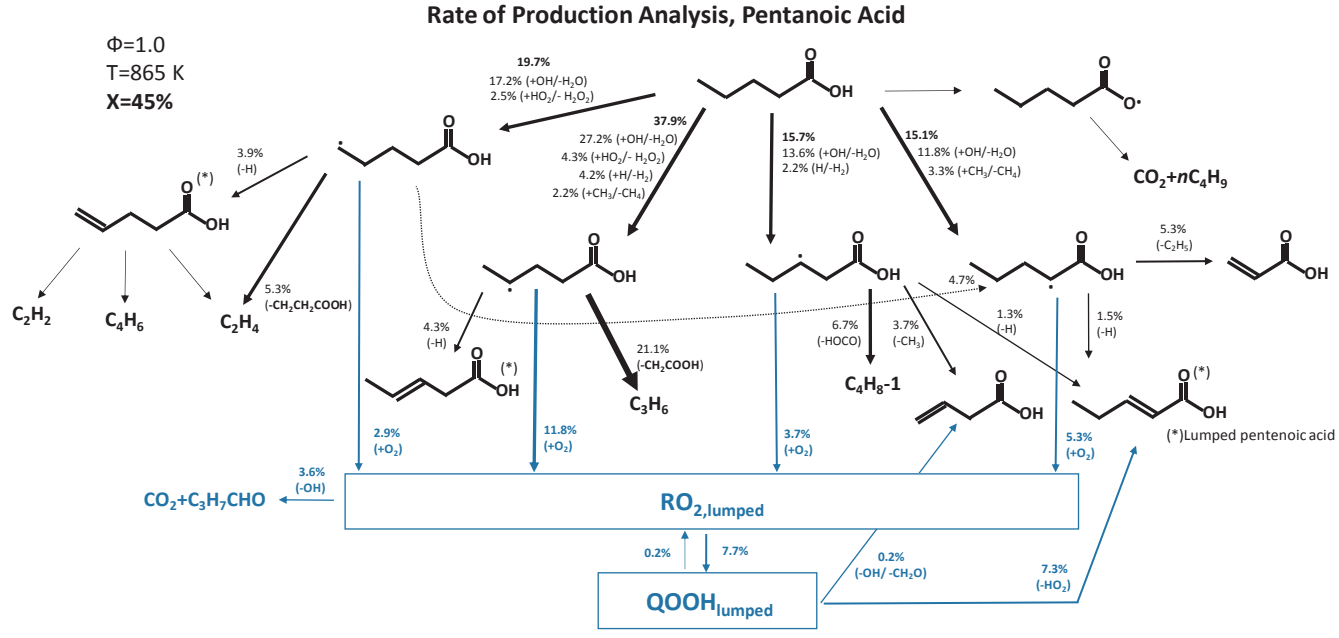

Fig. 14. Rate of production analysis of 0.5% pentanoic acid/O_2/N_2 oxidation at T = 865 K, φ = 1.0 and 45% conversion. Threshold for contribution is 2% flux.

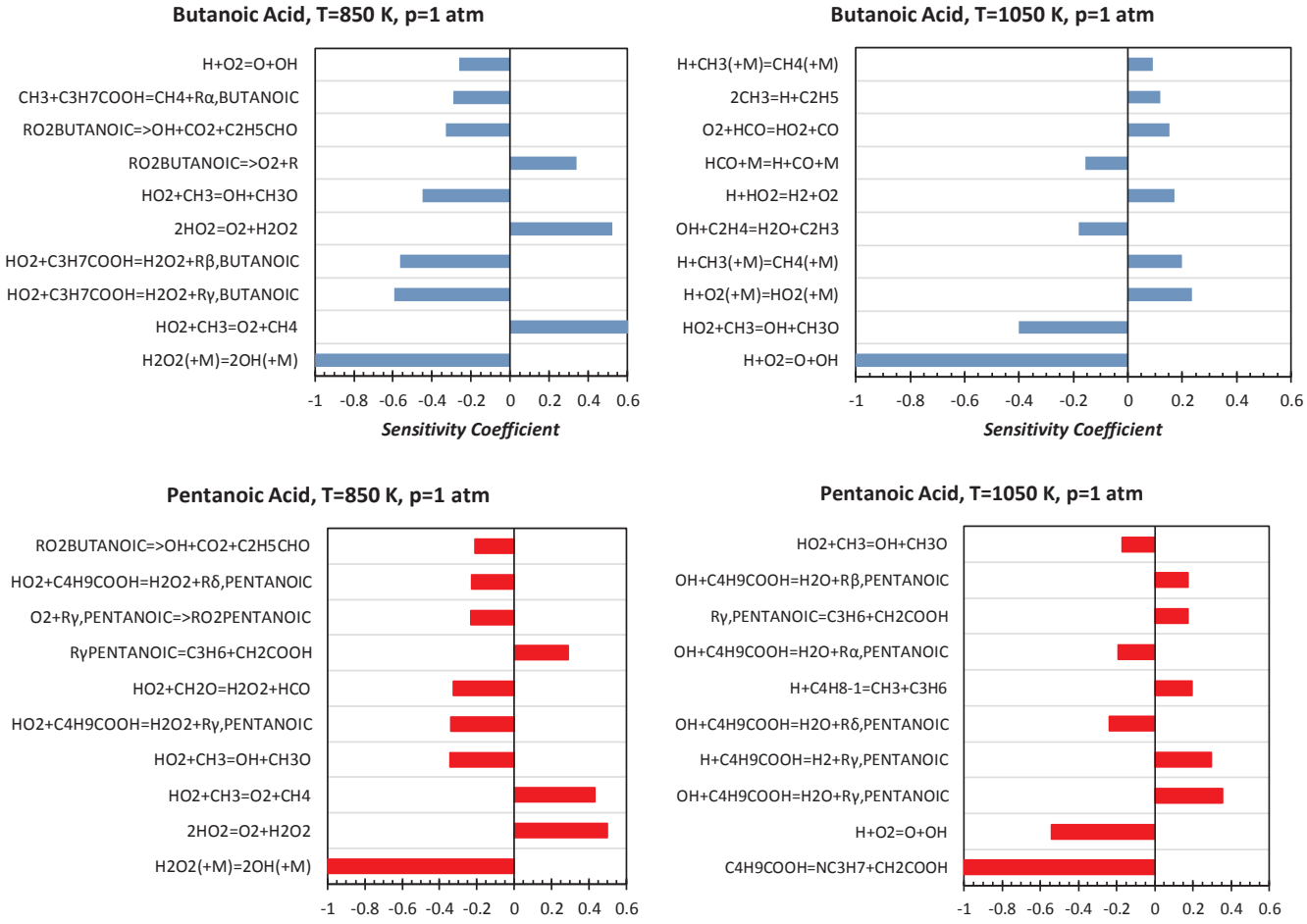

Fig. 15. Normalized sensitivity coefficients of fuel consumption to rate constants at T = 850 K (left) and 1050 K (right). Top panels (blue bars): butanoic acid, bottom panels (red bars): pentanoic acid.

and H. Also in pentanoic acid oxidation, only one lumped unsaturated pentenoic acid is considered as a representative for all the isomers. 1-butene (C4H8-1) is mostly formed by the decomposition of β–radical. Propenoic acid is the main decomposition product of the resonance stabilized α-radical. 23.7% of the overall fuel radical concentration undergo addition to O_2, forming RO_2. The longer carbon chain favors the isomerization to QOOH compared to butanoic acid, however most of QOOH is decomposed to form butenoic or pentenoic acids and does not propagate the low temperature branching.

Fig. 15 shows results from sensitivity analysis of fuel consumption to rate constants for butanoic and pentanoic acids, at two different temperatures T = 850 K and T = 1050 K. For both acids, at the lowest temperature, the reactivity is controlled by H_2O_2 decomposition to form two OH radicals H_2O_2 is produced by HO_2 radicals termination and by H-abstraction on the fuel by HO_2, also highlighted as sensitive reactions. The main source of HO_2 is for both fuels the decomposition of QOOH radicals to form unsaturated acids. H-abstractions by methyl on the α-site are also found to be important for butanoic acid. Methyl radical is mostly produced by the decomposition of $*CH_2{-}(C{=}O){-}OH$ forming CO_2 [17] and by the decomposition of α-radical forming propenoic acid. Interestingly, the Waddington-type mechanism producing propanal (C_2H_5CHO) in butanoic acid is also found to promote reactivity in pentanoic acid. The formation of butanoic radicals in pentanoic acid oxidation is related to the interactions of HO_2 with butenoic acid ($HO_2 + C_3H_5COOH = O_2 + R_{\alpha,butanoic}$). Concerning pentanoic acid oxidation at 850 K, it is interesting to note that the decomposition of $R_{\gamma,pentanoic}$ producing propene and $*CH_2{-}(C{=}O){-}OH$ radical decreases the reactivity forming one stable radical and propylene, that is mostly oxidized forming resonance stabilized allyl radical. At higher temperatures (T = 1050 K) butanoic acid is dominated by reactions belonging to the core kinetic model (C_0-C_2) while H-abstractions by OH dominate pentanoic acid reactivity.

6. Conclusion

This paper reports the first kinetic study of the oxidation of two large carboxylic acids, butanoic and pentanoic acids. Carboxylic acids are significant components in bio-oils obtained from biomass fast-pyrolysis, however the kinetics underlying their oxidation has not been addressed in the literature. In this study, experiments were performed using an atmospheric jet-stirred reactor at temperatures from 800 to 1100 K. A new detailed kinetic model was developed considering the specificities induced by the presence of the acid function. Kinetic pathways involving the remaining part of the molecule have been described according to rate rules for alkanes. The model thus obtained can reproduce the experimental data reasonably well, but some deviations are still observed. In particular, the model seems to predict a slower conversion of pentanoic acid at stoichiometric and rich conditions. The systematic approach here reported for butanoic and pentanoic acids has been recently applied successfully to investigate the kinetics of oxidation of other families of oxygenated molecules such as aldehydes and alcohols [6,9]. This study develops upon a recent theoretical study on acetic acid pyrolysis and oxidation and constitutes a further step in the attempt to advance the understanding of the kinetic effect of the carboxylic substitutions. Additional experimental data on the pyrolysis and high temperature oxidation (e.g. laminar flame speeds, ignition delay

times) of acetic, propanoic and higher molecular weight acids would be highly beneficial to this aim.

Acknowledgements

The authors acknowledge the financial support of IMPROOF project (H2020-IND-CE-2016-17/H2020-SPIRES016) European Union's Horizon 2020 research and innovation program (grant agreement no. 723706) and of the COST Action CM1404 “Chemistry of smart energy carriers and technologies - SMARTCATs”.

Appendix A. Supplementary data

Supplementary data to this article can be found online at https://doi.org/10.1016/j.cej.2019.05.090.

References

[1] A. Oasmaa, Y. Solantausta, V. Arpiainen, E. Kuoppala, K. Sipilä, Fast pyrolysis bio-oils from wood and agricultural residues, Energy Fuels 24 (2010) 1380–1388, https://doi.org/10.1021/ef901107f.
[2] M. Bertero, G. de la Puente, U. Sedran, Fuels from bio-oils: bio-oil production from different residual sources, characterization and thermal conditioning, Fuel 95 (2012) 263–271, https://doi.org/10.1016/j.fuel.2011.08.041.
[3] K. Onarheim, Y. Solantausta, J. Lehto, Process simulation development of fast pyrolysis of wood using aspen plus, Energy Fuels 29 (2015) 205–217, https://doi.org/10.1021/ef502023y.
[4] S.M. Sarathy, P. Oßwald, N. Hansen, K. Kohse-Höinghaus, Alcohol combustion chemistry, Prog. Energy Combust. Sci. 44 (2014) 40–102, https://doi.org/10.1016/j.pecs.2014.04.003.
[5] M. Pelucchi, C. Cavallotti, E. Ranzi, A. Frassoldati, T. Faravelli, Relative reactivity of oxygenated fuels: alcohols, aldehydes, ketones, and methyl esters, Energy Fuels 30 (2016) 8665–8679, https://doi.org/10.1021/acs.energyfuels.6b01171.
[6] M. Pelucchi, M. Bissoli, C. Rizzo, Y. Zhang, K. Somers, A. Frassoldati, H.J. Curran, T. Faravelli, A kinetic modelling study of alcohols operating regimes in a HCCI engine, SAE Int. J. Engines 10 (2017), https://doi.org/10.4271/2017-24-0077.
[7] M. Pelucchi, E. Ranzi, A. Frassoldati, T. Faravelli, Alkyl radicals rule the low temperature oxidation of long chain aldehydes, Proc. Combust. Inst. 36 (2017) 393–401, https://doi.org/10.1016/j.proci.2016.05.051.
[8] A. Rodriguez, O. Herbinet, F. Battin-Leclerc, A study of the low-temperature oxidation of a long chain aldehyde: n-hexanal, Proc. Combust. Inst. 36 (2017) 365–372, https://doi.org/10.1016/j.proci.2016.05.047.
[9] M. Pelucchi, S. Namysl, E. Ranzi, A. Frassoldati, O. Herbinet, F. Battin-Leclerc, T. Faravelli, An experimental and kinetic modelling study of n-C4C6 aldehydes oxidation in a jet-stirred reactor, Proc. Combust. Inst. (2018), https://doi.org/10.1016/j.proci.2018.07.087.
[10] O. Herbinet, F. Battin-Leclerc, S. Bax, H. Le Gall, P.-A. Glaude, R. Fournet, Z. Zhou, L. Deng, H. Guo, M. Xie, F. Qi, Detailed product analysis during the low temperature oxidation of n-butane, Phys. Chem. Chem. Phys. PCCP 13 (2011) 296–308, https://doi.org/10.1039/c0cp00539h.
[11] M. Cord, B. Husson, J.C. Lizardo Huerta, O. Herbinet, P.-A. Glaude, R. Fournet, B. Sirjean, F. Battin-Leclerc, M. Ruiz-Lopez, Z. Wang, M. Xie, Z. Cheng, F. Qi, Study of the low temperature oxidation of propane, J. Phys. Chem. A 116 (2012) 12214–12228, https://doi.org/10.1021/jp309821z.
[12] M. Cord, B. Sirjean, R. Fournet, A. Tomlin, M. Ruiz-Lopez, F. Battin-Leclerc, Improvement of the modeling of the low-temperature oxidation of n-butane: study of the primary reactions, J. Phys. Chem. A 116 (2012) 6142–6158, https://doi.org/10.1021/jp211434f.
[13] E. Ranzi, C. Cavallotti, A. Cuoci, A. Frassoldati, M. Pelucchi, T. Faravelli, New reaction classes in the kinetic modeling of low temperature oxidation of n-alkanes, Combust. Flame 162 (2015) 1679–1691, https://doi.org/10.1016/j.combustflame.2014.11.030.
[14] M. Christensen, A.A. Konnov, Laminar burning velocity of acetic acid + air flames, Combust. Flame 170 (2016) 12–29, https://doi.org/10.1016/j.combustflame.2016.05.007.
[15] M. Christensen, E.J.K. Nilsson, A.A. Konnov, A systematically updated detailed kinetic model for CH2O and CH3OH combustion, Energy Fuels 30 (2016) 6709–6726, https://doi.org/10.1021/acs.energyfuels.6b00049.
[16] F. Battin-Leclerc, A.A. Konnov, J.L. Jaffrezo, M. Legrand, To better understand the formation of short-chain acids in combustion systems, Combust. Sci. Technol. 180 (2007) 343–370, https://doi.org/10.1080/00102200701740782.
[17] C. Cavallotti, M. Pelucchi, A. Frassoldati, Analysis of acetic acid gas phase reactivity: rate constant estimation and kinetic simulations, Proc. Combust. Inst. (2018), https://doi.org/10.1016/j.proci.2018.06.137.
[18] CRECK Modeling - Home, (n.d.). http://creckmodeling.chem.polimi.it/ (accessed December 14, 2018).
[19] J.C. Mackie, K.R. Doolan, High-temperature kinetics of thermal decomposition of acetic acid and its products, Int. J. Chem. Kinet. 16 (1984) 525–541, https://doi.org/10.1002/kin.550160504.
[20] N. Leplat, J. Vandooren, Numerical and experimental study of the combustion of acetic acid in laminar premixed flames, Combust. Flame 159 (2012) 493–499, https://doi.org/10.1016/j.combustflame.2011.08.007.
[21] N. Sebbar, J. Appel, H. Bockhorn, Ketene formation through interaction reactions during P2O3/P2O5/CH3C(=O)OH pyrolysis, Combust. Sci. Technol. 188 (2016) 745–758, https://doi.org/10.1080/00102202.2016.1139376.
[22] K.R. Doolan, J.C. Mackie, C.R. Reid, High temperature kinetics of the thermal decomposition of the lower alkanoic acids, Int. J. Chem. Kinet. 18 (1986) 575–596, https://doi.org/10.1002/kin.550180508.
[23] J.M. Clark, M.R. Nimlos, D.J. Robichaud, Comparison of unimolecular decomposition pathways for carboxylic acids of relevance to biofuels, J. Phys. Chem. A 118 (2014) 260–274, https://doi.org/10.1021/jp4095485.
[24] J. Mendes, C.-W. Zhou, H.J. Curran, Theoretical chemical kinetic study of the H-Atom abstraction reactions from aldehydes and acids by Ḣ atoms and ȮH, HȮ2, and ĊH3 radicals, J. Phys. Chem. A 118 (2014) 12089–12104, https://doi.org/10.1021/jp5072814.
[25] E. Ranzi, A. Frassoldati, A. Stagni, M. Pelucchi, A. Cuoci, T. Faravelli, Reduced kinetic schemes of complex reaction systems: fossil and biomass-derived transportation fuels, Int. J. Chem. Kinet. 46 (2014) 512–542, https://doi.org/10.1002/kin.20867.
[26] A. Rodriguez, O. Herbinet, Z. Wang, F. Qi, C. Fittschen, P.R. Westmoreland, F. Battin-Leclerc, Measuring hydroperoxide chain-branching agents during n-pentane low-temperature oxidation, Proc. Combust. Inst. 36 (2017) 333–342, https://doi.org/10.1016/j.proci.2016.05.044.
[27] O. Herbinet, G. Dayma, Jet-stirred reactors, Clean. Combust. Springer, London, 2013, pp. 183–210, , https://doi.org/10.1007/978-1-4471-5307-8_8.
[28] O. Herbinet, F. Battin-Leclerc, Progress in understanding low-temperature organic compound oxidation using a jet-stirred reactor, Int. J. Chem. Kinet. 46 (2014) 619–639, https://doi.org/10.1002/kin.20871.
[29] O. Herbinet, P.-A. Glaude, V. Warth, F. Battin-Leclerc, Experimental and modeling study of the thermal decomposition of methyl decanoate, Combust. Flame 158 (2011) 1288–1300, https://doi.org/10.1016/j.combustflame.2010.11.009.
[30] Topaz GC Inlet Liners Page / Restek.com, (n.d.). https://www.restek.com/Landing-Pages/Topaz-GC-Inlet-Liners-Page (accessed December 14, 2018).
[31] Sample Loops, Sulfinert Treated / Sample Handling/Chromatography Products at Restek.com, (n.d.). https://www.restek.com/catalog/view/2352/22848 (accessed December 14, 2018).
[32] C. Muller, V. Michel, G. Scacchi, G.M. Côme, THERGAS: a computer program for the evaluation of thermochemical data of molecules and free radicals in the gas phase, J. Chim. Phys. Phys.-Chim. Biol. 92 (1995) 1154–1178.
[33] S.W. Benson, F.R. Cruickshank, D.M. Golden, G.R. Haugen, H.E. O'Neal, A.S. Rodgers, R. Shaw, R. Walsh, Additivity rules for the estimation of thermochemical properties, Chem. Rev. 69 (1969) 279–324, https://doi.org/10.1021/cr60259a002.
[34] K.A. Heufer, S.M. Sarathy, H.J. Curran, A.C. Davis, C.K. Westbrook, W.J. Pitz, Detailed kinetic modeling study of n-Pentanol oxidation, Energy Fuels 26 (2012) 6678–6685, https://doi.org/10.1021/ef3012596.
[35] Y.-R. Luo, Comprehensive Handbook of Chemical Bond Energies, CRC Press, 2007.
[36] E.T. Denisov, V.E. Tumanov, Estimation of the bond dissociation energies from the kinetic characteristics of liquid-phase radical reactions, Russ. Chem. Rev. 74 (2005) 825, https://doi.org/10.1070/RC2005v074n09ABEH001177.
[37] E. Ranzi, M. Dente, T. Faravelli, G. Pennati, Prediction of kinetic parameters for hydrogen abstraction reactions, Combust. Sci. Technol. 95 (1993) 1–50, https://doi.org/10.1080/00102209408935325.
[38] M.G. Evans, M. Polanyi, Further considerations on the thermodynamics of chemical equilibria and reaction rates, Trans. Faraday Soc. 32 (1936) 1333–1360, https://doi.org/10.1039/TF9363201333.
[39] E. Ranzi, M. Dente, A. Goldaniga, G. Bozzano, T. Faravelli, Lumping procedures in detailed kinetic modeling of gasification, pyrolysis, partial oxidation and combustion of hydrocarbon mixtures, Prog. Energy Combust. Sci. 27 (2001) 99–139, https://doi.org/10.1016/S0360-1285(00)00013-7.
[40] W.K. Metcalfe, S.M. Burke, S.S. Ahmed, H.J. Curran, A hierarchical and comparative kinetic modeling study of C1–C2 hydrocarbon and oxygenated fuels, Int. J. Chem. Kinet. 45 (2013) 638–675.
[41] S.M. Burke, W. Metcalfe, O. Herbinet, F. Battin-Leclerc, F.M. Haas, J. Santner, F.L. Dryer, H.J. Curran, An experimental and modeling study of propene oxidation. Part 1: speciation measurements in jet-stirred and flow reactors, Combust. Flame 161 (2014) 2765–2784, https://doi.org/10.1016/j.combustflame.2014.05.010.
[42] E. Ranzi, A. Frassoldati, R. Grana, A. Cuoci, T. Faravelli, A.P. Kelley, C.K. Law, Hierarchical and comparative kinetic modeling of laminar flame speeds of hydrocarbon and oxygenated fuels, Prog. Energy Combust. Sci. 38 (2012) 468–501, https://doi.org/10.1016/j.pecs.2012.03.004.
[43] W. Pejpichestakul, E. Ranzi, M. Pelucchi, A. Frassoldati, A. Cuoci, A. Parente, T. Faravelli, Examination of a soot model in premixed laminar flames at fuel-rich conditions, Proc. Combust. Inst. (2018), https://doi.org/10.1016/j.proci.2018.06.104.
[44] M. Pelucchi, C. Cavallotti, A. Cuoci, T. Faravelli, A. Frassoldati, E. Ranzi, Detailed kinetics of substituted phenolic species in pyrolysis bio-oils, React. Chem. Eng. (2018), https://doi.org/10.1039/C8RE00198G.
[45] B. Ruscic, Uncertainty quantification in thermochemistry, benchmarking electronic structure computations, and Active Thermochemical Tables, Int. J. Quantum Chem. 114 (2014) 1097–1101, https://doi.org/10.1002/qua.24605.
[46] A. Burcat, B. Ruscic, Chemistry, T.-I.I. of Tech, Third Millenium Ideal Gas and Condensed Phase Thermochemical Database for Combustion (With Update from Active Thermochemical Tables), Argonne National Lab. (ANL), Argonne, IL (United States), 2005, , https://doi.org/10.2172/925269.
[47] A. Cuoci, A. Frassoldati, T. Faravelli, E. Ranzi, OpenSMOKE++: an object-oriented

framework for the numerical modeling of reactive systems with detailed kinetic mechanisms, Comput. Phys. Commun. 192 (2015) 237–264, https://doi.org/10.1016/j.cpc.2015.02.014.
[48] D.J.M. Ray, D.J. Waddington, Gas phase oxidation of alkenes—Part II. The oxidation of 2-methylbutene-2 and 2,3-dimethylbutene-2, Combust. Flame 20 (1973) 327–334, https://doi.org/10.1016/0010-2180(73)90024-2.
[49] O. Welz, J.D. Savee, A.J. Eskola, L. Sheps, D.L. Osborn, C.A. Taatjes, Low-temperature combustion chemistry of biofuels: pathways in the low-temperature (550–700K) oxidation chemistry of isobutanol and tert-butanol, Proc. Combust. Inst. 34 (2013) 493–500, https://doi.org/10.1016/j.proci.2012.05.058.